ACS NANO

www.acsnano.org

ARTICLE

Fluorine-Free Ion-Selective Membrane with Enhanced Mg^{2+} Transport for Mg-Organic Batteries

Wen Ren, Migo Szeman Ng, Ye Zhang, Alae Eddine Lakraychi, Yanliang Liang, Dawei Feng, Michelle Lehmann, Guang Yang, Judith Jeevarajan, Wan Si Tang,* and Yan Yao*

Cite This: *ACS Nano* 2025, 19, 5781−5788

Read Online

ACCESS | Metrics & More | Article Recommendations | Supporting Information

ABSTRACT: **Magnesium batteries offer a safer alternative for next-generation battery technology due to their insusceptibility to dendrite deposition. Selective membranes tailored for magnesium-ion conduction will unlock further technological advancement. Herein, we demonstrate fluorine-free magnesiated sulfonated poly(ether ether ketone) (Mg-SPEEK) selective membranes capable of facilitating magnesium-ion conduction while effectively rejecting soluble organic species. These membranes demonstrate a reversible Mg plating and stripping Coulombic efficiency (CE) of 85.4% and an ionic conductivity of 3.3 × 10^{-4} S cm^{-1} at room temperature, surpassing those for a Mg-Nafion selective membrane. Theoretical density functional theory (DFT) calculations reveal that SPEEK possesses more localized charge centers along its backbone compared with Nafion, potentially facilitating enhanced ion conduction. Full cells assembled with Mg-SPEEK coupled with the organic cathode pyrene-4,5,9,10-tetraone (PTO) and Mg metal demonstrated significantly improved capacity retention as compared to those assembled with conventional nonselective separators.**

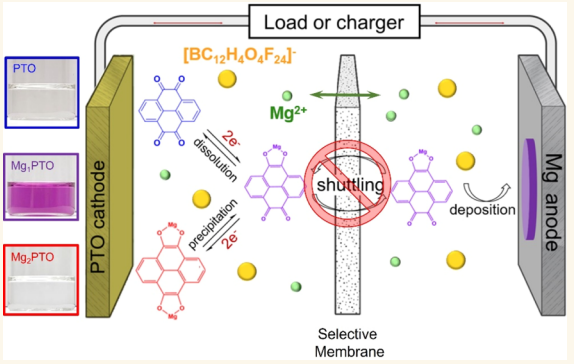

KEYWORDS: *ion-selective membrane, fluorine-free, magnesium batteries, organic cathode, ionic conductivity, optical characterization*

INTRODUCTION

Rechargeable magnesium batteries (RMBs) are a promising next-generation battery technology due to the earth abundance, high theoretical volumetric capacity, and dendrite-free deposition of magnesium.[1,2] When coupled with organic cathode materials, Mg-organic batteries provide faster reaction kinetics as Mg^{2+} exhibits weaker coordination with the organic anion host and higher power density through a heterogeneous "solid−liquid−solid" enolization conversion chemistry.[3] In addition, their transition-metal-free nature is cost-effective and sustainable.[4,5] Mg-organic batteries are associated with capacity degradation due to the diffusion of partially soluble redox intermediates. It is important to leverage the fast heterogeneous redox kinetics of organic intermediates while maintaining their conversion reversibility.[6,7] Strategies to enhance the cyclability of Mg-organic batteries include tuning the organic molecular structures, polymerizing small organic molecules, and modifying electrolytes.[8−10] In addition, separator engineering is also considered an effective and facile strategy to inhibit intermediates' diffusion. For example, traditional polyolefin or glass fiber (GF) separators with functional coating layers, such as graphene oxide (GO) and poly(vinylpyrrolidone)-modified graphene, have been demonstrated to impede the migration of soluble Mg-organic species.[3,11] The downside of these separators is that they contain pores of varying sizes in the micrometer range, and their ability to block small organic intermediates over extended periods selectively still remains a challenge requiring further optimization. Covalent organic framework (COF)-based bilayer membrane has also been explored and demonstrated promising rejection capability due to their high density of aligned nanopores.[12] Nonetheless, the fabrication process relies on interfacial polymerization requiring a long reaction time and stable liquid−liquid interface.

Received: December 8, 2024
Revised: January 18, 2025
Accepted: January 22, 2025
Published: January 29, 2025

Scheme 1. Schematic of Mg-PTO Cells and the Function of the Separator and Membrane[a]

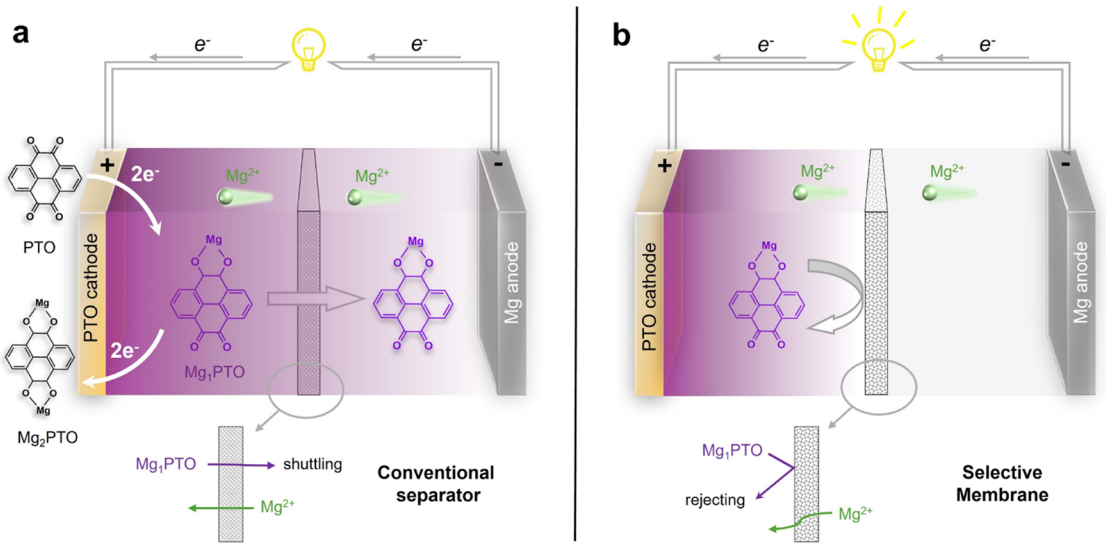

[a](a) Conventional separator used in Mg-PTO cells leads to the shuttle effect of the liquefied Mg_1PTO intermediate. (b) Selective membranes are employed to address this issue by preventing the diffusion of the Mg_1PTO intermediate.

An alternative strategy of separator engineering is to utilize cation exchange membranes (CEMs), which exhibit excellent chemical stability and functional groups to address this shuttling issue, by blocking organic intermediates on the cathode side while conducting only the Mg^{2+} cation. While lithiated and sodiated perfluorosulfonated membranes have improved the cycling stability of Li/Na−S and Li-organic batteries,[13−15] cation-selective membranes tailored for RMBs remain relatively understudied. Matsumoto et al. recently demonstrated the feasibility of magnesiated Nafion-based membranes when swollen with the solution of magnesium bis(trifluoromethanesulfonyl)imide ($Mg(TFSI)_2$) in triglyme.[16] However, the Coulombic efficiency (CE) of Mg stripping and plating was poor, likely due to multiple Mg-passivating components in the system. The inherently Mg-passivating anions such as $TFSI^-$ and trifluoromethanesulfonate (OTf^-) are unsuitable for achieving stable Mg-organic batteries.[17] Moreover, the interfacial stability between Nafion and metallic magnesium may prove challenging considering the reactivity of organic fluorides.[18]

Herein, we report a fluorine-free sulfonated poly(ether ether ketone) (SPEEK)-based ion-selective membrane, which, when combined with the magnesium tetrakis-(hexafluoroisopropyloxy)borate ($Mg[B(hfip)_4]_2$, MBF) electrolyte, reaches a high ionic conductivity of 3.3×10^{-4} S cm^{-1} at room temperature. The membrane enables a reversible Mg stripping and plating CE of 85.36% and a selective rejection of soluble magnesium-organic redox intermediates like magnesium pyrene-4,5,9,10-tetraone (Mg_1PTO) and magnesium 5,5′-dimethyl-2,2′-bis-*p*-benzoquinone (Mg_1MBBQ). Mg-PTO full cells assembled with Mg-SPEEK showed improved cycling stability and lower overpotential compared with those assembled with Mg-Nafion. Scheme 1 illustrates the Mg-organic cells during operation by using (a) a conventional separator and (b) a selective membrane. The schematics demonstrate that the conventional separator allows the dissolved Mg_1PTO intermediate to shuttle between the cathode and the anode. In contrast, the selective membrane effectively prevents diffusion of the intermediate, thereby eliminating shuttling.

RESULTS AND DISCUSSION

Fabrication of Magnesiated Membranes. Scheme 2 illustrates the typical membrane treatment procedure using commercial CEMs, such as Nafion or SPEEK. These membranes were magnesiated through cationic exchange of the initial proton or potassium cations by ebullition in an aqueous $MgCl_2$ solution. Vacuum drying was subsequently performed at 150 °C to ensure complete water removal.

Scheme 2. Cation Exchange during the Magnetization Process

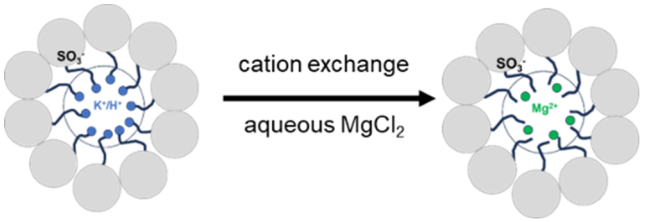

Figure 1 illustrates the molecular structure and scanning electron microscopy (SEM)/energy-dispersive X-ray (EDX) analyses of Mg-SPEEK and Mg-Nafion. The cross-sectional SEM images of Mg-SPEEK and Mg-Nafion reveal a dense morphology with no visible micron-scale pores. Due to its physical confinement properties, this structure could selectively block small organic molecules. The EDX elemental analyses indicate that the atomic ratio of magnesium to sulfur is approximately 1:2, consistent with the polymeric structure. In this structure, each divalent Mg^{2+} is embedded between two sulfonate groups. Nafion membranes have been widely reported to contain nanoscale channels with 4−5 nm pores in aqueous systems.[19] The nanopores and negatively charged sulfonate groups along the side chains are distinct structural features that inhibit the transport of charged organic intermediates. The magnesiated membranes are soaked and

https://doi.org/10.1021/acsnano.4c17740
ACS Nano 2025, 19, 5781−5788

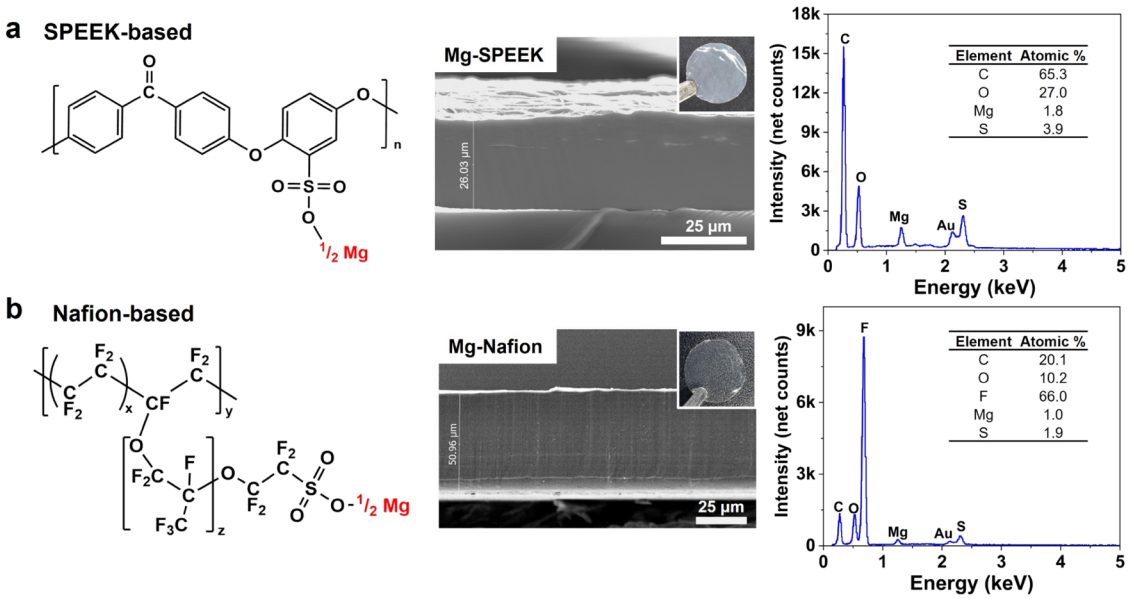

Figure 1. Chemical structures and physical characterizations of Mg-selective membranes. (a) Polymeric unit of the magnesiated SPEEK structure and cross-sectional SEM images with its corresponding EDX spectra (Mg-E620PE). (b) Polymer unit of the magnesiated Nafion membrane and cross-sectional SEM images with its corresponding EDX spectra (Mg-N212). Insets are optical images of the membranes.

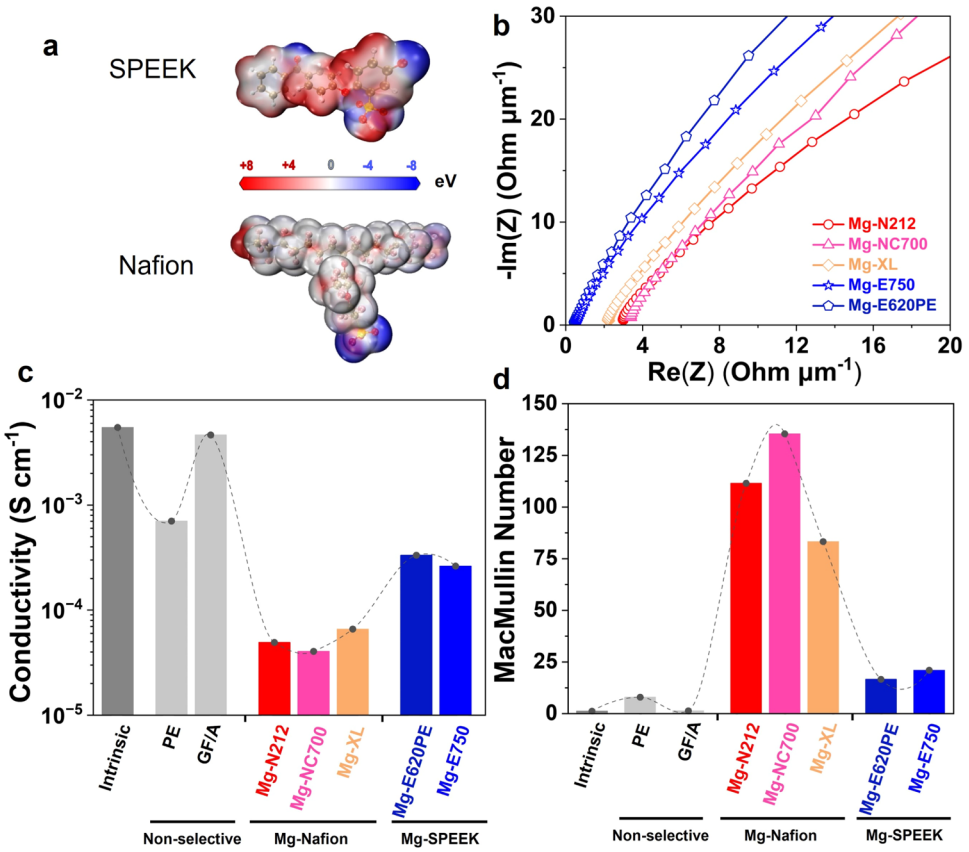

Figure 2. Transport properties of Mg-selective membranes. (a) Electrostatic potential (ESP) isosurfaces of SPEEK and Nafion molecules. (b) Normalized electrochemical impedance spectroscopy (EIS) of the symmetric SS|membrane|SS Swagelok cells. (c) Ionic conductivities and (d) MacMullin numbers of different membranes. The intrinsic value is the ionic conductivity of the electrolyte, where 0.3 M MBF 1,2-dimethoxyethane (DME)/diglyme (G2) is used. Mg-N212, Mg-NC700, and Mg-XL are Nafion-based, and Mg-E620PE and Mg-E750 are SPEEK-based.

swollen in a liquid electrolyte, during which solvent molecules chelate with Mg^{2+}, leading to proposed membrane structural changes illustrated in Figure S1a.

The FTIR spectra shown in Figure S1b compare the functional group changes with the pristine membranes; the magnesiation pretreatment did not change the characteristic IR

https://doi.org/10.1021/acsnano.4c17740
ACS Nano 2025, 19, 5781−5788

peaks, indicating a good consistency of the polymer structure in both Mg-Nafion and Mg-SPEEK. One of the most important peaks is located around 1700 cm^{-1}, corresponding to the sulfonate group chelated to cations. In Mg-Nafion, the original −OH bending signal at 1692 cm^{-1} shifts to a lower wavenumber of 1645 cm^{-1} after magnesiation, indicating proton replacement, a phenomenon commonly observed in Li-Nafion membranes.[20] In Mg-SPEEK, the characteristic peaks corresponding to the sulfonate group chelated with pristine potassium ions show no significant shift upon replacement with Mg^{2+}. In this regard, the SPEEK membrane demonstrates good universal structural compatibility with both monovalent and multivalent cations.

Transport Properties of Magnesiation Membranes. One critical parameter for evaluating the transport properties of a selective membrane is the MacMullin number, defined as the ratio of the membrane's resistivity to that of the permeating liquid electrolyte.[21] A high MacMullin number implies that the membrane significantly hinders Mg^{2+} transport, which is undesirable for high-performance ion-selective applications. Herein, we first compared the MacMullin number of different types of separators commonly used in RMBs under consistent test conditions. The setup and protocol for measuring the ionic conductivity with and without separators are depicted in Figure S2. Theoretical density functional theory (DFT) calculations were performed to establish the relationship between the microscopic chemical structure and ionic conduction, as shown in Figure 2a. Despite the high electronegativity of the fluorine atoms, the symmetrical C−F bonds along the Nafion backbone result in a delocalized charge distribution, as shown in the electrostatic potential (ESP) isosurfaces. The optimized Nafion molecule exhibits a nearly neutral charge along the backbone with a negative charge concentrated on the sulfonate groups, the primary chelating sites for Mg^{2+}. In contrast, the ESP isosurface of SPEEK shows that the negative charge is mainly concentrated on the oxygen atoms connecting the aromatic rings. This localization of charge centers increases the dipole moment, which provides a lower migration barrier for the positively charged Mg^{2+} cation. The strategy of modifying the chemical environment of charged groups, such as by adjusting pendant groups with varying hydrophobicities, has been shown to effectively regulate hydration-restrained pores and ionic conductivities.[22] We also conducted the swelling test of both Mg-N212 and Mg-E750 membranes at room temperature. As shown in Figure S3, the results indicate a final thickness increase of ∼6−7%. No strong correlation was observed between the transport properties and the swelling ratios for membranes.

The four-point electrochemical impedance spectroscopy (EIS) measurement, utilizing ion-blocking electrodes (e.g., SS electrode), is a simple and widely used method for determining electrolyte conductivity.[23] In Figure 2b, the EIS spectra for Mg-selective membranes were normalized to eliminate the impact of the membrane thickness on resistance. The membranes within the same category (Mg-N212, Mg-XL, Mg-NC700 for Mg-Nafion and Mg-E750, Mg-E620PE for Mg-SPEEK) show highly overlapping curves and similar bulk resistance, demonstrating that the intrinsic resistivity of Mg-SPEEK membrane is lower than that of Mg-Nafion. The ionic conductivities and corresponding MacMullin numbers of the swollen membrane are summarized in Figure 2c,d and Tables S2 and S3. Traditional GF and polyethylene (PE) separators retained better ionic conductivities, decreasing from 5.5 mS cm^{-1} (intrinsic) to 4.6 and 0.7 mS cm^{-1}, respectively. However, the MacMullin number of Mg-N212 (Nafion-based) is 111, with a conductivity of only 4.9×10^{-5} S cm^{-1}, indicating that the conductivity retention of the Mg-N212 membrane swollen with the electrolyte is less than 1%. In contrast, at the same thickness of 50 μm, the MacMullin number of Mg-E750 (SPEEK-based) is significantly lower at 21 with a corresponding order of magnitude higher conductivity at 2.61×10^{-4} S cm^{-1}, demonstrating a more favorable Mg^{2+} transport through the Mg-SPEEK selective membrane.

Although Mg-SPEEK exhibits ionic conductivity higher than that of Mg-Nafion, its MacMullin number remains higher than that of conventional separators such as GF and polyolefin, leading to slower transport and thus posing a challenge for high-rate battery cycling applications. This disparity is likely attributed to the different ion transport mechanisms between ion-selective membranes and conventional separators. Conventional separators rely on physical pores for ion transport, isolating electrode electrons while allowing the entire electrolyte liquid to pass through.[24] Consequently, factors such as porosity, pore size distribution, and tortuosity directly influence the MacMullin number of these separators.[25] As the SEM images show in Figure S5, the glass fiber separator, with the highest porosity (89.1%), retains over 84% of its Mg electrolyte ionic conductivity. Cellulose and poly(vinylidene difluoride) (PVDF) membranes with a medium porosity exhibit around 25% ionic conductivity retention. In contrast, the PE separator retains only 12.8% conductivity, corresponding to a MacMullin number of 7.8. The densest trilayer PP/PE/PP separator has a MacMullin number exceeding 12.

Permeability Tests of Mg-Organic Intermediate. The key criterion for evaluating a selective membrane's effectiveness is its ability to block soluble Mg-organic intermediates. A practical method involves a diffusion-driven concentration permeability test to evaluate the membrane's rejection capability. A soluble organic intermediate, Mg_1MBBQ, is chosen rather than Mg_1PTO because of the easy chemical synthesis and ability to chemically magnesiate. The MBBQ precursor was synthesized by following ref 26. Figure 3 compares diffusion suppression over time, illustrating the diffusion of Mg_1MBBQ through PE, GO-coated PE, Mg-Nafion, and Mg-SPEEK membranes. To minimize the potential impact of membrane thickness on the permeability of soluble intermediates, we chose Mg-N212 and Mg-E750 membranes, both with a thickness of 50 μm, as the control samples. A concentration gradient of 0.01 M was used to observe the crossover of the black Mg_1MBBQ solution from the right to the left. The PE separator showed the least effectiveness in inhibiting diffusion, with significant diffusion recorded after just 1 h. The GO surface coating layer reduced the permeability of the PE separator, but noticeable darkening still occurred within 7 h. In contrast, the Mg-Nafion and Mg-SPEEK membranes demonstrated significantly better isolation, showing no visible diffusion at 10 h. Remarkably, the left chamber remained clear and transparent even after 3 days, indicating that the selective membranes effectively block the diffusion of Mg_1MBBQ intermediates.

Electrochemistry of Mg-Selective Membrane. The stability of selective membranes to conduct Mg^{2+} under high electric field conditions in actual batteries is crucial for its application in practical Mg-organic full cells. An asymmetric Mg|Cu cell was first assembled to study the Mg stripping and

https://doi.org/10.1021/acsnano.4c17740
ACS Nano 2025, 19, 5781−5788

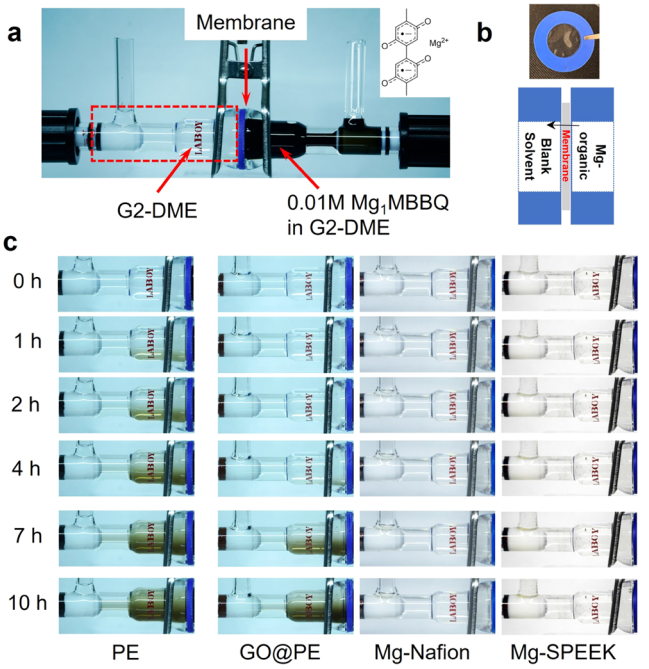

Figure 3. Selective capability of Mg-selective membranes. (a) H-cell setup for measuring Mg_1MBBQ diffusion. (b) Schematic illustration of the crossover region. (c) Ex situ optical comparison demonstrating diffusion suppression. GO@PE: PE separator with a 10 μm thick surface GO coating. Mg-Nafion and Mg-SPEEK refer to Mg-N212 and Mg-E750, respectively.

plating behavior, as shown in Figure S9a,b. In a typical cell with a GF separator, a CE of over 96.9% could be achieved under 5 mA cm^{-2} and 5 mAh cm^{-2}, with an overpotential of 240 mV. Mg-Nafion demonstrates unstable Mg stripping and plating behavior in Figure S10c, with a low overall CE of 51.2%. Encouragingly, Mg-SPEEK shows a stable voltage profile and an improved CE of 85.4%. Compared with Mg-Nafion, Mg-SPEEK demonstrates a lower overpotential of 200 mV at the same current density of 0.05 mA cm^{-2}, which could be explained by its higher Mg^{2+} ionic conductivity.

Figure 4 illustrates the stability of the Mg-PTO full cells. Given the high McMullin number of selective membranes, thinner membranes (Mg-E620PE and Mg-NC700) were utilized in the electrochemical tests to reduce membrane impedance while effectively blocking the shuttle of Mg_1PTO. The cell with the GF separator experienced rapid capacity decay, with discharge capacity decreasing to 220 mAh g^{-1} after five cycles. In contrast, the cell with Mg-Nafion showed improved cycling stability over the first five cycles. The capacity stabilized at approximately 360 mAh g^{-1} after the first cycle. The significant polarization observed with Mg-Nafion is consistent with its inherently low ionic conductivity. Mg-SPEEK demonstrated an effective capacity utilization of 407 mAh g^{-1} in the initial cycle and exhibited excellent stability compared to GF. Furthermore, Mg-SPEEK exhibited a lower polarization than Mg-Nafion in the Mg|PTO full cell, indicating its superior transport property.

In Situ Optical Characterization with Mg-SPEEK Membrane. The distinct purple color of the Mg_1PTO intermediate allows optical characterization to be an effective technique for studying its diffusion evolution upon cycling. To better understand the inhibition effect of Mg-SPEEK membranes in actual batteries, a specialized EL-Cell was designed for in situ optical monitoring. Figure 5a illustrates the

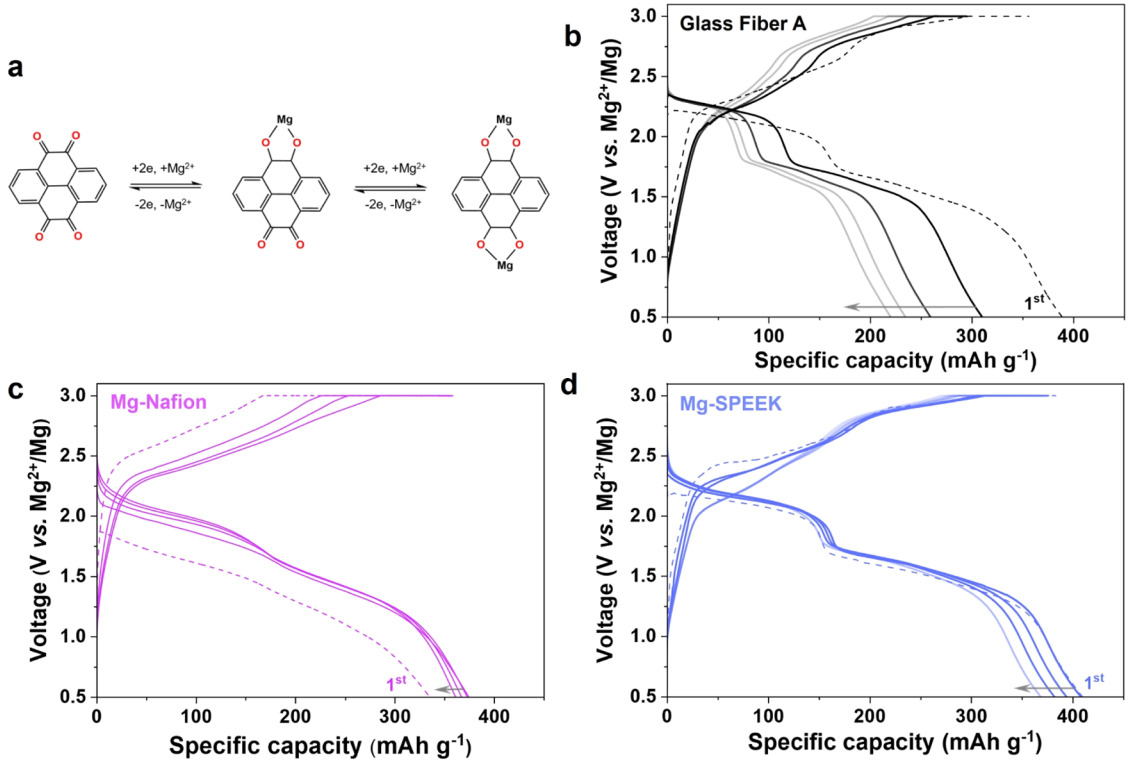

Figure 4. Mg|PTO full cells cycling with different membranes. (a) Redox reaction pathway of PTO. Electrochemical curve with (b) glass fiber-A, (c) Mg-NC700, and (d) Mg-E620PE membranes as the separator. The cycling rate is C/2 (1C = 408 mA g^{-1}). The dotted line represents the first cycle, with the arrows indicating the progression from the second to the fifth cycle.

https://doi.org/10.1021/acsnano.4c17740
ACS Nano 2025, 19, 5781−5788

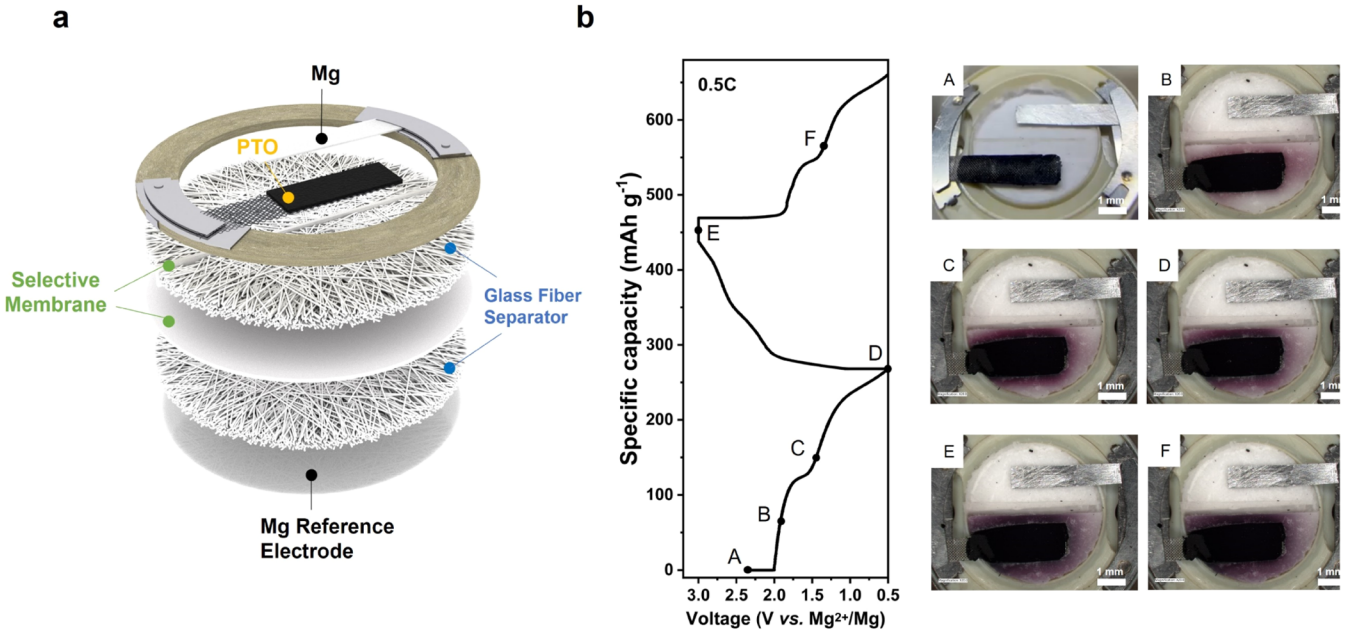

Figure 5. In situ optical characterization of a Mg|PTO full cell with the Mg-SPEEK (Mg-E620PE) selective membrane. (a) Schematic EL-Cell structure of optical characterization. (b) Electrochemical curve and representative snapshots during cycling.

EL-Cell structure, in which GF was used to retain the electrolyte separated by the Mg-SPEEK membranes. The upper GF was divided into two parts, corresponding to the Mg anode and PTO cathode compartment, respectively. Encased between two glass fiber separators, the sandwiched Mg-SPEEK membrane is designed to prevent passivation of the bottom reference Mg electrode by shuttled soluble Mg_1PTO. Figure 5b illustrates the representative snapshot of the cell cycling, and the video is shown in Video S1. At the beginning of discharge (point B), the purple Mg_1PTO intermediate dissolves, coloring the entire electrolyte purple. This process corresponds to the conversion of insoluble PTO into soluble Mg_1PTO. The dissolution process peaks at the end of the first plateau (point C). As the discharge continues, Mg_1PTO precipitates as Mg_2PTO, and the color of the electrolyte gradually becomes lighter (point D). Upon recharging (point E), the purple color around the electrode fades. A new dissolution process begins during the subsequent discharge cycle (point F). Leveraging the diffusion−rejection capability of the Mg-SPEEK membrane, the colored Mg_1PTO intermediate is effectively confined to the cathode region, preventing crossover to the Mg side.

CONCLUSIONS

In summary, a fluorine-free Mg-SPEEK selective membrane capable of facilitating Mg-ion conduction while effectively rejecting soluble organic species has been developed. The Mg-SPEEK membrane, when swollen with the MBF electrolyte, demonstrates a higher ionic conductivity of 3.3×10^{-4} S cm^{-1} at room temperature and a reversible Mg stripping and plating CE of 85.4% in the Mg|Cu cell. Theoretical DFT calculations suggest that the higher ionic conductivity of SPEEK, compared to that of Nafion, may result from the presence of localized charge centers along its backbone. The Mg-SPEEK membrane significantly inhibits the diffusion of organic intermediates and is broadly applicable to Mg-organic intermediates such as Mg_1MBBQ and Mg_1PTO. The Mg|PTO full cell assembled with Mg-SPEEK demonstrated considerably improved cycling stability and reduced overpotential. In situ optical characterization confirmed the selective membrane's effectiveness in blocking the shuttling of the organic Mg_1PTO intermediate. Overall, this fluorine-free selective Mg-SPEEK membrane presents a promising approach to improving the stability of Mg-organic batteries.

METHODS

Materials. Nafion membranes (N212, XL, and NC700) and SPEEK membranes (K-E750 and K-E620PE) were purchased from Chemours and Fumapem, respectively. $NaBH_4$ (98%) was purchased from Alfa Aesar. 1,1,1,3,3,3-Hexafluoro-2-propanol (99.5%) was purchased from Aladdin Scientific. 1,2-Dimethoxyethane (DME), diglyme (G2), and $MgCl_2$ (anhydrous, 98%), ammonium cerium nitrate (98.5%), and Mg powders (99%) were purchased from Sigma-Aldrich. $Mg(TFSI)_2$ (99.5%, Solvionic) was dried in a Buchi vacuum oven at 150 °C for 24 h prior to use. Mg foil (99.9%, 100 μm) was supplied by MTI. 2,5-Dimethoxytoluene (98%) was purchased from TCI. Pyrene-4,5,9,10-tetraone (PTO) was sourced from Solarmer Beijing Ltd., and 5,5′-dimethyl-2,2′-bis-*p*-benzoquinone (MBBQ) was synthesized from the previously reported procedure.[26] The MBBQ and Mg powders were stirred in the DME:G2 mixture solvent and reacted inside a glovebox for 2 weeks to synthesize the Mg_1MBBQ intermediate. All solvents were stored with activated 3-Å molecular sieves until the moisture was below 5 ppm, tested by Karl Fischer titration. Mg foil was polished with sandpaper before use, and Cu foil was washed with acetone before use. PTO, Ketjenblack carbon (KB), and PTFE binder were mixed in a 3:5:2 mass ratio using isopropyl alcohol as a medium and then pressed onto the SS316 mesh current collector. The areal mass loading of PTO was approximately 1.0 mg cm^{-2}. Fabricated cathodes were dried at 60 °C under a vacuum overnight.

Fabrication of Magnesiated Membranes. Pristine Nafion and SPEEK membranes were immersed into a 0.1 M aqueous $MgCl_2$ solution at 80 °C for 2 h with stirring to ensure that the counterions were saturated and exchanged with Mg^{2+}. After this, it was washed with ultrapure water to remove excess $MgCl_2$. The magnesiated membranes were vacuum-dried at 150 °C for 24 h before being stored in the Ar-filled glovebox. Unless otherwise indicated, the selective membranes were swollen inside the 0.3 M MBF DME/G2 electrolyte overnight before cell assembly.

https://doi.org/10.1021/acsnano.4c17740
ACS Nano 2025, 19, 5781−5788

Preparation of Electrolyte. $[Mg{\cdot}3DME][B(hfip)_4]_2$ (MBF) salt was synthesized from previous reports.[27] $Mg(BH_4)_2$ was synthesized by the displacement reaction of $Na(BH_4)_2$ and $MgCl_2$ under diethyl ether reflux condition.[28] Briefly, premixed hexafluoroisopropyl alcohol/DME was slowly added dropwise to a stoichiometric $Mg(BH_4)_2$/DME solution and stirred overnight. The excess DME solvent was removed by rotary evaporation (85 °C, 35 hPa). The resulting white MBF powder was dissolved in a DME/G2 solvent mixture (1:1 volume ratio) to obtain the 0.3 M MBF DME/G2 electrolyte. In a typical preparation of 0.75 M $Mg(TFSI)_2$/DME electrolyte, a measured amount of $Mg(TFSI)_2$ powder was added to the DME solvent and stirred overnight to obtain a clear solution.

Material Characterization. Scanning electron microscopy (SEM), energy-dispersive X-ray (EDX) diffraction spectrum, and elemental mapping were carried out with an AxiaChemi. Membranes were gold-sputtered before SEM and EDX. Fourier transform infrared (FTIR) measurements were conducted with a Nicolet iS5 with the reflection model. A 500 MHz nuclear magnetic resonance (NMR) spectrometer (JEOL, model ECA-500) was utilized. All chemical shift values (δ) are expressed in parts per million relative to tetramethylsilane (TMS). Dimethyl sulfoxide (DMSO)-d_6 was used as the deuterated solvent to dissolve the MBF salt fully. The proton spectrum with a 0.4−10 ppm range was conducted to verify the MBF salt purity. The EL-CELL (ECC-Opto-10) and Keyence (VHX-7000N) digital microscopes were utilized for in situ optical characterization. The working electrode and counter electrode were assembled in side-by-side mode.

Ionic Conductivity Measurement. A Swagelok cell setup was assembled to quantify the ionic conductivity. For bulky electrolyte conductivity, a nonflooding amount of 100 μL of electrolyte was injected into a PTFE O-ring with a known thickness (L) and inner area (S). The ionic conductivity could be calculated as follows

$$\sigma = \frac{L}{R_b S}$$

R_b is the resistance of the bulk solution, which could be measured by electrochemical impedance spectroscopy (EIS). A four-probe testing was used to delete the contact impedance. The detailed setup structure and description are given in Figure S2 and the corresponding notes. All conductivity measurements were conducted at room temperature (23 °C).

Electrochemical Measurements. All electrochemical measurements were conducted with the Swagelok cells in an Ar-filled glovebox (MBraun, <0.5 ppm of water and oxygen) and tested at room temperature unless otherwise indicated. The galvanostatic charge−discharge and electrochemical impedance spectroscopy (EIS) of assembled cells were performed on a potentiostat (VMP3, Bio-Logic). EIS frequency was conducted from 1 MHz to 0.1 Hz. Glass fiber/A (Whatman) separators were used for galvanostatic charge−discharge. In the asymmetric Mg|Cu half-cell, the Mg (diameter 9.6 mm) was counter to the Cu foil (diameter 10 mm). The Aurbach protocol for accurately determining electrolyte CE% was followed in the Mg|Cu cell.[29]

DFT Calculations. The Nafion and SPEEK molecular have been optimized at B3LYP and the 6-311 G(d,p) basis set by the Gaussian 16 package.[30] Frequency calculation was performed at the same level to confirm that imaginary frequency is absent. The quantitative molecular surface analysis of electrostatic potential (ESP) was performed with the Multiwfn package.[31] Visualization of theoretical calculations was conducted by visual molecular dynamics (VMD).[32]

ASSOCIATED CONTENT

Supporting Information

The Supporting Information is available free of charge at https://pubs.acs.org/doi/10.1021/acsnano.4c17740.

Experimental setups and additional characterizations, including FTIR, SEM, and NMR (PDF)

Operando optical video (Video S1) (MP4)

AUTHOR INFORMATION

Corresponding Authors

Wan Si Tang − *Electrochemical Safety Research Institute (ESRI), UL Research Institutes, Houston, Texas 77204, United States;* orcid.org/0000-0002-7893-3025; Email: wansi.tang@ul.org

Yan Yao − *Department of Electrical and Computer Engineering and Texas Center for Superconductivity at the University of Houston, University of Houston, Houston, Texas 77204, United States;* orcid.org/0000-0002-8785-5030; Email: yyao4@central.uh.edu

Authors

Wen Ren − *Department of Chemical and Biomolecular Engineering, University of Houston, Houston, Texas 77204, United States;* orcid.org/0000-0002-1461-6717

Migo Szeman Ng − *Electrochemical Safety Research Institute (ESRI), UL Research Institutes, Houston, Texas 77204, United States*

Ye Zhang − *LiBeyond LLC, Houston, Texas 77023, United States*

Alae Eddine Lakraychi − *Department of Electrical and Computer Engineering and Texas Center for Superconductivity at the University of Houston, University of Houston, Houston, Texas 77204, United States*

Yanliang Liang − *LiBeyond LLC, Houston, Texas 77023, United States;* orcid.org/0000-0001-6771-5172

Dawei Feng − *Department of Materials Science and Engineering, University of Wisconsin−Madison, Madison, Wisconsin 53706, United States;* orcid.org/0000-0002-6285-850X

Michelle Lehmann − *Chemical Sciences Division, Oak Ridge National Laboratory, Oak Ridge, Tennessee 37831, United States*

Guang Yang − *Chemical Sciences Division, Oak Ridge National Laboratory, Oak Ridge, Tennessee 37831, United States;* orcid.org/0000-0003-0583-6272

Judith Jeevarajan − *Electrochemical Safety Research Institute (ESRI), UL Research Institutes, Houston, Texas 77204, United States;* orcid.org/0000-0003-4843-7597

Complete contact information is available at: https://pubs.acs.org/10.1021/acsnano.4c17740

Notes

The authors declare the following competing financial interest(s): Y.Y. has an equity interest in LiBeyond, LLC and Solid Design Instruments, LLC. The University of Houston reviewed and approved the relationship in compliance with its conflict-of-interest policy. The remaining authors declare no competing interests.

ACKNOWLEDGMENTS

Y.Y. acknowledges the funding support from the UL Research Institutes (No. 1177365).

REFERENCES

(1) Liang, Y. L.; Dong, H.; Aurbach, D.; Yao, Y. Current status and future directions of multivalent metal-ion batteries. *Nat. Energy* **2020**, *5* (9), 646−656.

(2) Zhang, J. L.; Chang, Z. Y.; Zhang, Z. H.; Du, A. B.; Dong, S. M.; Li, Z. J.; Li, G. C.; Cui, G. L. Current Design Strategies for Rechargeable Magnesium-Based Batteries. *ACS Nano* **2021**, *15* (10), 15594−15624.

(3) Dong, H.; Tutusaus, O.; Liang, Y. L.; Zhang, Y.; Lebens-Higgins, Z.; Yang, W. L.; Mohtadi, R.; Yao, Y. High-power Mg batteries enabled by heterogeneous enolization redox chemistry and weakly coordinating electrolytes. *Nat. Energy* **2020**, *5* (12), 1043−1050.
(4) Bitenc, J.; Pirnat, K.; Luzanin, O.; Dominko, R. Organic Cathodes, a Path toward Future Sustainable Batteries: Mirage or Realistic Future? *Chem. Mater.* **2024**, *36* (3), 1025−1040.
(5) He, X. Q.; Cheng, R. Q.; Sun, X. Y.; Xu, H.; Li, Z.; Sun, F. Z.; Zhan, Y.; Zou, J. X.; Laine, R. M. Organic cathode materials for rechargeable magnesium-ion batteries: Fundamentals, recent advances, and approaches to optimization. *J. Magnesium Alloys* **2023**, *11* (12), 4359−4389.
(6) Poizot, P.; Gaubicher, J.; Renault, S.; Dubois, L.; Liang, Y. L.; Yao, Y. Opportunities and Challenges for Organic Electrodes in Electrochemical Energy Storage. *Chem. Rev.* **2020**, *120* (14), 6490−6557.
(7) Chen, Y.; Fan, K.; Gao, Y. B.; Wang, C. L. Challenges and Perspectives of Organic Multivalent Metal-Ion Batteries. *Adv. Mater.* **2022**, *34* (52), No. 2200662.
(8) Song, X. M.; Xue, X. L.; Xia, H. L.; Jin, L.; Tao, A. Y.; Wang, Y. D.; Liang, J. C.; Liu, Y. Z.; Zhang, P. B.; Tie, Z. X.; Long, Y. T.; Jin, Z. Electrolyte initiated instaneous chemical polymerization of organic cathodes for ultralong-cycling magnesium ion batteries. *Energy Storage Mater.* **2023**, *55*, 426−435.
(9) Pan, B. F.; Huang, J. H.; Feng, Z. X.; Zeng, L.; He, M. N.; Zhang, L.; Vaughey, J. T.; Bedzyk, M. J.; Fenter, P.; Zhang, Z. C.; Burrell, A. K.; Liao, C. Polyanthraquinone-Based Organic Cathode for High-Performance Rechargeable Magnesium-Ion Batteries. *Adv. Energy Mater.* **2016**, *6* (14), No. 1600140.
(10) Cui, L. M.; Zhou, L. M.; Zhang, K.; Xiong, F. Y.; Tan, S. S.; Li, M. S.; An, Q. Y.; Kang, Y. M.; Mai, L. Q. Salt-controlled dissolution in pigment cathode for high-capacity and long-life magnesium organic batteries. *Nano Energy* **2019**, *65*, No. 103902.
(11) Xue, X. L.; Huang, T. L.; Zhang, Y.; Zhong, Q. J.; Tang, M. K.; Shang, H.; Zhang, Y. X.; Cui, M. S.; Qi, J. Q.; Xu, H.; Sui, Y. W. Synergy of electrolyte manipulation and separator functionalization enables ultralong-life nonaqueous magnesium-organic batteries. *J. Mater. Chem. A* **2024**, *12* (37), 24955−24965.
(12) Lakraychi, A. E.; Picton, E. S.; Liang, Y.; Shaffer, D. L.; Yao, Y. Suppressing Shuttle Effect with a Size-Selective Covalent Organic Framework Based Bilayer Membrane. *ACS Energy Lett.* **2023**, *8* (12), 5032−5040.
(13) Huang, J. Q.; Zhang, Q.; Peng, H. J.; Liu, X. Y.; Qian, W. Z.; Wei, F. Ionic shield for polysulfides towards highly-stable lithium-sulfur batteries. *Energy Environ. Sci.* **2014**, *7* (1), 347−353.
(14) Song, Z. P.; Qian, Y. M.; Otani, M.; Zhou, H. S. Stable Li-Organic Batteries with Nafion-Based Sandwich-Type Separators. *Adv. Energy Mater.* **2016**, *6* (7), No. 1501780.
(15) Yu, X. W.; Manthiram, A. Ambient-Temperature Sodium-Sulfur Batteries with a Sodiated Nafion Membrane and a Carbon Nanofiber-Activated Carbon Composite Electrode. *Adv. Energy Mater.* **2015**, *5* (12), No. 1500350.
(16) Okuo, T.; Mandai, T.; Masunaga, H.; Ohta, N.; Matsumoto, H. Magnesiated Nafion-Based Gel Electrolytes: Structural and Electrochemical Characterization. *J. Phys. Chem. C* **2023**, *127* (29), 14502−14509.
(17) Shea, J. J.; Luo, C. Organic Electrode Materials for Metal Ion Batteries. *ACS Appl. Mater. Interfaces* **2020**, *12* (5), 5361−5380.
(18) Häcker, J.; Rommel, T.; Lange, P.; Zhao-Karger, Z.; Morawietz, T.; Biswas, I.; Wagner, N.; Nojabaee, M.; Friedrich, K. A. Magnesium Anode Protection by an Organic Artificial Solid Electrolyte Interphase for Magnesium-Sulfur Batteries. *ACS Appl. Mater. Interfaces* **2023**, *15* (27), 33013−33027.
(19) Schmidt-Rohr, K.; Chen, Q. Parallel cylindrical water nanochannels in Nafion fuel-cell membranes. *Nat. Mater.* **2008**, *7* (1), 75−83.
(20) Yu, X. W.; Joseph, J.; Manthiram, A. Polymer lithium-sulfur batteries with a Nafion membrane and an advanced sulfur electrode. *J. Mater. Chem. A* **2015**, *3* (30), 15683−15691.
(21) Landesfeind, J.; Hattendorff, J.; Ehrl, A.; Wall, W. A.; Gasteiger, H. A. Tortuosity Determination of Battery Electrodes and Separators by Impedance Spectroscopy. *J. Electrochem. Soc.* **2016**, *163* (7), A1373−A1387.
(22) Wang, A.; Breakwell, C.; Foglia, F.; Tan, R.; Lovell, L.; Wei, X.; Wong, T.; Meng, N.; Li, H.; Seel, A.; et al. Selective ion transport through hydrated micropores in polymer membranes. *Nature* **2024**, *635* (8038), 353−358.
(23) Cooper, K. R. Progress Toward Accurate Through-Plane Ion Transport Resistance Measurement of Thin Solid Electrolytes. *J. Electrochem. Soc.* **2010**, *157* (11), B1731−B1739.
(24) Lagadec, M. F.; Zahn, R.; Müller, S.; Wood, V. Topological and network analysis of lithium ion battery components: the importance of pore space connectivity for cell operation. *Energy Environ. Sci.* **2018**, *11* (11), 3194−3200.
(25) Lagadec, M. F.; Zahn, R.; Wood, V. Characterization and performance evaluation of lithium-ion battery separators. *Nat. Energy* **2019**, *4* (1), 16−25.
(26) Yokoji, T.; Kameyama, Y.; Maruyama, N.; Matsubara, H. High-capacity organic cathode active materials of 2,2′-bis-benzoquinone derivatives for rechargeable batteries. *J. Mater. Chem. A* **2016**, *4* (15), 5457−5466.
(27) Zhao-Karger, Z.; Bardaji, M. E. G.; Fuhr, O.; Fichtner, M. A new class of non-corrosive, highly efficient electrolytes for rechargeable magnesium batteries. *J. Mater. Chem. A* **2017**, *5* (22), 10815−10820.
(28) Yang, J.; Zheng, J.; Zhang, X.; Li, Y.; Yang, R.; Feng, Q.; Li, X. Low-temperature mass production of superconducting MgB2 nanofibers from Mg(BH4)2 decomposition and recombination. *Chem. Commun.* **2010**, *46* (40), 7530−7532.
(29) Adams, B. D.; Zheng, J. M.; Ren, X. D.; Xu, W.; Zhang, J. G. Accurate Determination of Coulombic Efficiency for Lithium Metal Anodes and Lithium Metal Batteries. *Adv. Energy Mater.* **2018**, *8* (7), No. 1702097.
(30) Frisch, M. J.et al. *Gaussian 16*, revision C.01; Gaussian, Inc.: Wallingford, CT, 2016.
(31) Lu, T.; Chen, F. Multiwfn: A multifunctional wavefunction analyzer. *J. Comput. Chem.* **2012**, *33* (5), 580−592.
(32) Humphrey, W.; Dalke, A.; Schulten, K. VMD: Visual molecular dynamics. *J. Mol. Graphics* **1996**, *14* (1), 33−38.

https://doi.org/10.1021/acsnano.4c17740
ACS Nano 2025, 19, 5781−5788